16TH EUROPEAN CONFERENCE ON EARTHQUAKE ENGINEERING THESSALONIKI 18 - 21 JUNE 2018

INFLUENCE OF NON-STRUCTURAL COMPONENTS ON THE SEISMIC RESPONSE OF COLD - FORMED STEEL STRUCTURES

Violetta NIKOLAIDOU[1], Colin A. ROGERS[2], Dimitrios G. LIGNOS[3]

ABSTRACT

Shortcomings exist with respect to accounting for the influence of non-structural components, e.g. gypsum panels installed on the ceilings (floors and roof diaphragms) and walls, on the response of cold-formed steel (CFS) framed structures subjected to seismic excitation. The current North American building codes and CFS related design standards (AISI S400 North American Standard for Seismic Design of Cold-Formed Steel Structural Systems & AISI S100 / CSA S136 North American Specification for the Design of Cold-Formed Steel Structural Members) do not take into account the diaphragms' contribution to the lateral resistance or stiffness of the structure, nor do they consider the contribution of the non-structural components found throughout the building. To improve on the seismic design of CFS structures, the CFS-NEES building, as tested by researchers at Johns Hopkins University, was chosen as a case study structure and modelled in the OpenSees platform, including interior non-structural gypsum sheathing and gravity walls. A 2D non-linear diaphragm model was initially created and, subsequently, incorporated in the 3D building model. The diaphragm model was calibrated based on a recently completed laboratory test program conducted at McGill University involving 9 cold-formed steel framed diaphragm configurations (16 diaphragm specimens) subjected to in-plane monotonic and reversed cyclic loading. Response history analyses revealed that, although interior gypsum panels increased the stiffness of the individual shear walls, the addition of gravity walls resulted in a reduction of the shear wall forces. The gravity walls contributed to the resistance of the lateral load. As the stiffness of the structure increased, the fundamental period and wall line inter-storey drift ratios decreased, and the total base shear increased in both directions, with the gravity walls being the dominant lateral force resisting elements.

Keywords: non-structural components; gypsum panels; diaphragm; gravity walls; OpenSees

1. INTRODUCTION

During the last decade, the seismic design of cold-formed steel (CFS) structures has been the focus of multi-university research projects, e.g. Dubina (2008), Fiorino et al. (2012), Yu & Li (2012), Shamim et at. (2013), Peterman (2014), Leng (2015), Padilla-Liano (2015), Florig et al. (2015), Chatterjee (2016), Accorti et al. (2016), and Nikolaidou et al. (2017), among others. The goal in North America is to improve the current design provisions (AISI S400 (2015) North American Standard for Seismic Design of Cold-Formed Steel Structural Systems & AISI S100 (2016) / CSA S136 (2016) North American Specification for the Design of Cold-Formed Steel Structural Members) by employing both experimental and numerical work. Although, numerous studies have already been conducted for the main lateral force resisting elements, the shear walls, e.g. Branston et al. (2006), Pan & Shan (2011), Liu et al. (2012) and Shamim (2012), among others; limited numerical and experimental work exists on the diaphragm's influence on the overall lateral response, as well as the influence of non-structural components (Florig et al. 2015, Chatterjee 2016, Nikolaidou et al. 2017); the contribution of these

[1]PhD Candidate, McGill University, Department of Civil Engineering and Applied Mechanics, Montreal, Canada, violetta.nikolaidou@mail.mcgill.ca
[2]Associate Professor, McGill University, Department of Civil Engineering and Applied Mechanics, Montreal, Canada, colin.rogers@mcgill.ca
[3]Associate Professor, Swiss Federal Institute in Lausanne (EPFL), School of Architecture, Civil & Environmental Engineering, Lausanne, Switzerland, dimitrios.lignos@epfl.ch

elements has yet to be established and included in the seismic design of multi-storey CFS structures.
A full-scale CFS building experiment was realized at Johns Hopkins University as part of a research program entitled "Enabling Performance-Based Seismic Design of Multi-Story Cold-Formed Steel Structures" (Peterman 2014). The full size two-storey CFS wood sheathed shear wall building was tested (CFS-NEES Building) under earthquake loading using the Network for Earthquake Engineering Simulation (NEES) equipment site (shake table) at the State University of New York (SUNY) at Buffalo in the USA. Shamim (2012) conducted incremental dynamic analyses (IDA) of archetype CFS structures including the one tested in Buffalo using a 3D numerical model in the OpenSees simulation platform (McKenna 1997) as part of the investigation of the seismic response of steel sheathed CFS framed shear wall structures. Pin-ended truss elements were used to simulate the walls with the Pinching4 material model (Lowes & Altoontash 2004). In Leng (2015), based on experimental work on shear walls conducted by Liu et al. (2012) and the numerical work of Shamim (2012), dynamic and non-linear response history analyses were conducted in order to simulate the response of the CFS-NEES Building using. The same simulation approach and experimental data as the shear walls was assumed for the floor and roof diaphragm simulation at the time.
Chatterjee (2016) conducted a pushover analysis of a 3D ABAQUS model of the floor subsystem in both directions, while Florig et al. (2015) tested the simply supported full-scale floor subsystem in the z-direction, only; both studies provided the monotonic lateral response of the floor diaphragm up to the peak load. Chatterjee, also, proposed an upper and lower bound for the lateral response considering perfect friction or no friction incorporated between the wood panels, respectively. In the summer of 2015 and the winter of 2016 a laboratory test program was completed in two phases at McGill University involving nine 3.66m × 6.1m cold-formed steel framed diaphragm configurations (16 diaphragm specimens) subjected to in-plane monotonic and reversed cyclic loading. The diaphragm configurations were based on the floor and roof subsystems of the CFS-NEES Building (Nikolaidou et al. 2017, Latreille 2016) and non-structural components such as gypsum panels ceiling and gypcrete flooring were considered. The importance of the non-structural components has been highlighted with respect to seismic performance, not only on a subsystem level but also on the overall response of the structure by numerous studies. Lu (2015) tested twenty-five shear walls during the summer of 2014 at McGill University under reversed cyclic loading involving one or two layers of 15.9mm gypsum placed on both sides of a wall. She showed that the two layers of gypsum lead to double the ultimate shear strength of the wall. Eight tests were also conducted on bearing walls with gypsum (no hold downs) revealing their lateral stiffness and capacity. Shamim & Rogers (2015) added a 12.5mm gypsum layer to the shear walls for two numerically simulated CFS structures assumed to be located in Montreal and Vancouver; they showed that there was an increase in their seismic performance. Peterman (2014) presented results for the CFS-NEES Building in various phases of construction (with and without non-structural panels for the walls and diaphragms) clearly showing the effect of non-structural gypsum panels in the period elongation as well as the shear force distribution when those panels are added to the gravity framing walls.
The work presented herein comprises an investigation of the effect of non-structural components in a subsystem level focusing on the diaphragm lateral response and, subsequently, on the overall seismic response of a CFS structure. Results for the diaphragm test configurations containing a non-structural gypsum ceiling and a gypcrete topping are summarized. The CFS-NEES Building is chosen as a case study and simulated in the OpenSees platform (McKenna 1997). Through response history analyses, the influence of the non-structural gypsum sheathing and gravity walls is quantified in terms of fundamental period, base shear distribution and general shear wall behaviour. A simplified approach is followed in modelling the CFS framing of the structure where half of the gravity framing is included in the model, while the experimental data obtained from the diaphragm test program at McGill University (Nikolaidou et al. 2017) are used for the simulation of the floor and roof subsystems.

2. EXPERIMENTAL WORK

This section includes a description of the results obtained for the 3.66m × 6.1m diaphragm test specimen configurations, including the non-structural gypsum ceiling and the gypcrete topping. Detailed information of this work can be found in Nikolaidou et al. (2017) and Latreille (2016).

2.1 Diaphragm Specimens and Test Set-Up

To accommodate the diaphragm experimental program a test set-up was designed and built at the Jamieson Structures Laboratory at McGill University, comprised of a self-reacting braced frame, a roller system as a support of a distribution beam to transfer the load from actuator to specimen and a fixed connection consisting of built-up I sections (Figures 1a and 1b). The cantilever test approach was followed. Table 1 provides the diaphragm specimen characteristics presented in this paper.

a) b)

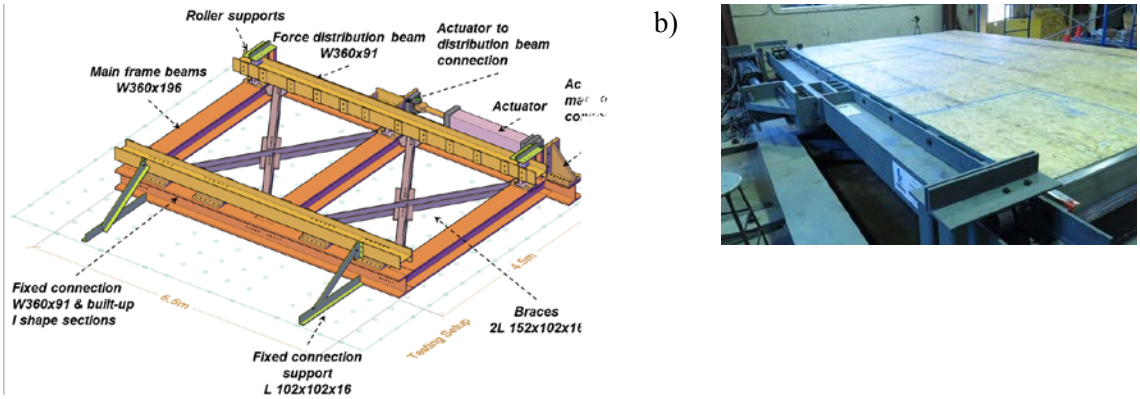

Figure 1. Diaphragm experimental program; a) test set-up, and b) specimen attached to test set-up

Table 1. Diaphragm specimens with non-structural components.

RGYP: Roof Diaphragm with 16mm gypsum panels ceiling/Unblocked*	**Section (mm) ASTM A653 (2015) Grade 50 steel**	**Length (mm)**
Joists	305S51-137M	3505
Rim Joists	305T51-173M	6480
Web Stiffeners	L 38×38×1.37	250
Joist bracing	305S41-137M	560
Joist bracing connectors	L 38×102×1.37	250
Straps	38×1.37	6300
#8 sheathing self-drilling (152/305mm spacing)	-	50
#10 steel-to-steel flat head self-drilling	-	20
#10 steel-to-steel Hex Head Cap self-drilling	-	25
OSB panels (24/16 rated)	2400×1200×11	-
FCRETE: Floor Diaphragm with 19mm gypcrete topping/Unblocked*	**Section (mm) ASTM A653 (2015) Grade 50 steel**	**Length (mm)**
Joists	350S64-246M	3505
Rim Joists	350T64-246M	6480
Web Stiffeners	L 38×38×1.37	280
Joist bracing	305S51-137M	550
Joist bracing connectors	L 38×102×1.37	250
Straps	38×1.37	6300
#12 sheathing self-drilling (152/305mm spc)	-	44
#10 steel-to-steel flat head self-drilling	-	20
#10 steel-to-steel Hex Head Cap self-drilling	-	25
OSB panels (48/24 rated T&G)	2400×1200×18	-

Note: *Unblocked: Fewer screws in the intermediate panel locations ; no steel underneath to attach all OSB panel edges

Configuration RGYP (Table 1) was tested under monotonic and reversed cyclic loading, while configuration FCRETE was tested only under monotonic loading. The CUREE displacement controlled loading protocol for ordinary ground motions (Krawinkler et al. 2000) was selected for the reversed cyclic tests following a displacement rate of 15mm/min, increased to 60mm/min after a level of 60mm of displacement was reached. For the monotonic loading case a displacement rate of 2.5mm/min for the roof and 5mm/min for the floor configuration was applied. The instrumentation employed involved linear variable differential transformers (LVDTs ±15 mm stroke) and string potentiometers (254 mm & 508 mm total stroke) in order to capture lateral displacement and shear deformation as well as local in-plane displacement, apart from the internal LVDT and load cell of the actuator.

2.2 Results

Results are presented in the form of a comparison for the same diaphragm configurations with and without the non-structural components. Figure 2a illustrates the lateral response of the RGYP specimen while Figure 2b refers to the FCRETE specimen.

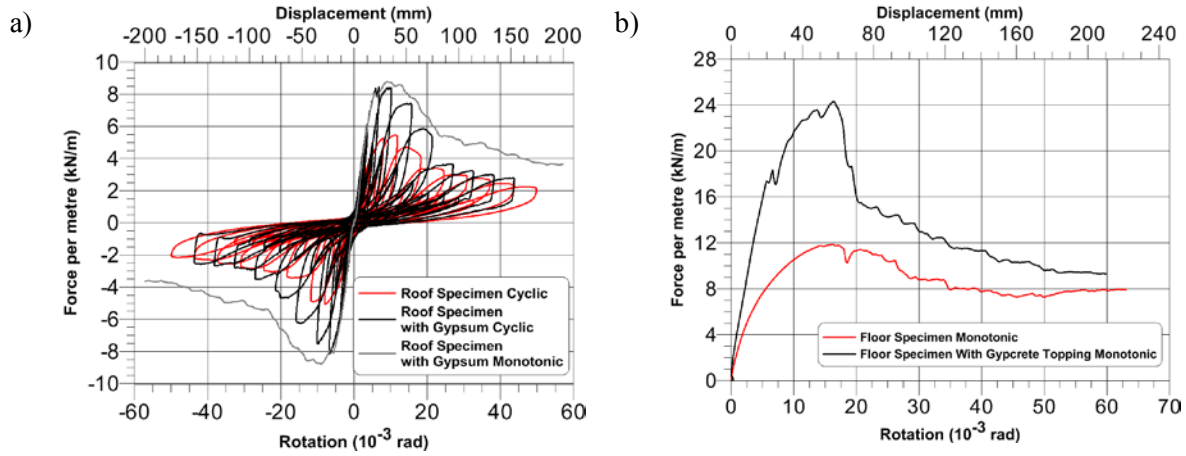

Figure 2. Lateral response; a) RGYP monotonic & cyclic loading, and b) FCRETE, monotonic loading

The addition of one layer of gypsum panels in the roof diaphragm configuration led to a 60% increase in shear strength and over a 100% increase in shear stiffness (Figure 2a). It is also shown that the monotonic and cyclic response of the RGYP specimen is similar up to the ultimate strength point, after which steeper strength degradation is observed, as expected, for the cyclic response due to the cumulative damage by the repetitive loading cycles. Prior to reaching peak load, for the RGYP specimen, shearing of the drywall screws (gypsum – to – framing connections) resulted in a small drop in shear strength; after peak load typical failure modes were observed for the OSB-to-framing connections such as the screws tearing out or pulling through the wood in the intermediate panel locations, as expected for an unblocked diaphragm configuration. Figure 3a demonstrates typical OSB screw failure modes and Figure 3b shows gypsum panels having completely disconnected after all drywall screws had failed (at peak load displacement level).

The addition of the gypcrete topping was beneficial, similar to the gypsum panels, leading to over a 100% increase in shear strength and stiffness for the floor configuration (Figure 2b). After installation, the gypcrete bonded with the OSB panels creating a considerably stronger composite material. After the test was completed, the only method that proved successful enough in order to be able to separate the two materials was to crush the gypcrete topping from above. During testing, the tension field that was developed in the diaphragm due to the in-plane lateral load caused cracking to occur perpendicular to the tensile forces (Figure 3c). The cracks slowly propagated separating the panels as shown in Figure 3d. The composite gypcrete / OSB material kept the sheathing screws in place, not allowing them to tilt, which resulted in a higher connection resistance and ultimate wood bearing and tear out failure of the sheathing-to-framing connections after considerable separation of the panels had occurred.

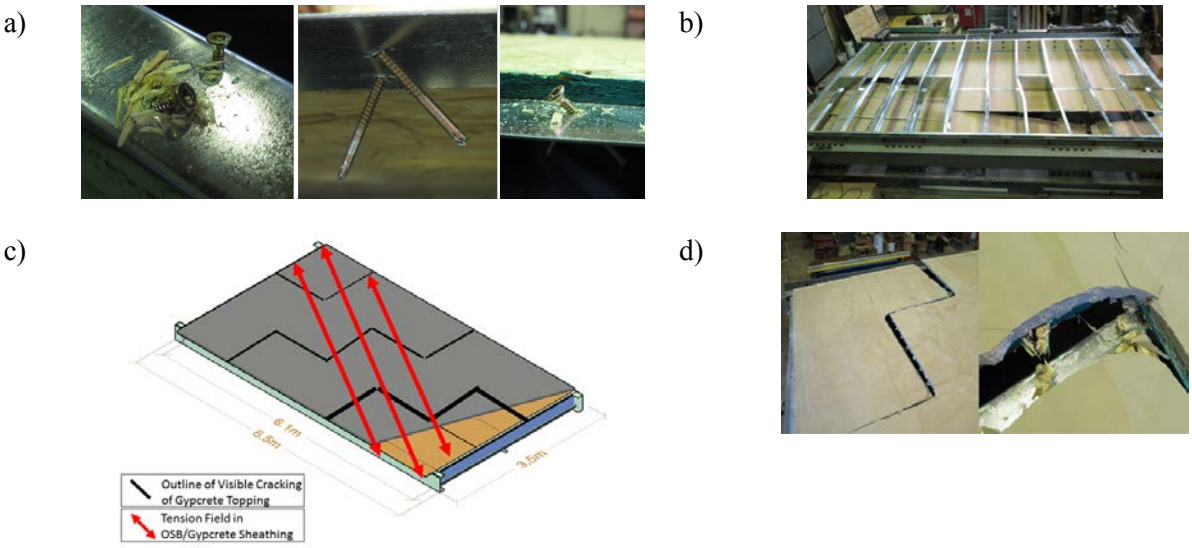

Figure 3. Failure modes; a) RGYP, typical screw failure modes, b) RGYP, separation of gypsum panels, c) FCRETE, gypcrete topping cracking and d) FCRETE, OSB panel separation and tear out failure of connections

3. NUMERICAL WORK

The CFS-NEES Building was chosen as a representative CFS structure, given the detailed experimental data available for its overall seismic response; a 7.01m × 15.16m structure with 2.74m storey height. Figure 4 shows the building modelled in the OpenSees platform (McKenna 1997). The modelling approach for each of the elements of the structure is also depicted in Figure 4 and explained in the following subsections of Section 3.

3.1 Shear walls and hold-down/chord stud connection

The numerical simulation of the shear walls is based on the modelling approach of Shamim (2012) (2D Model). For each wall a pair of truss elements is used and Pinching4 parameters (Lowes & Altoontash 2003) are inserted as material properties (as provided by Leng (2015)). The material properties are calibrated using experimental data from Liu et al. (2012) Tests 4 & 14 with wall widths of 1.22m and 2.44m, respectively and 2.74m height, following the exact same framing and sheathing characteristics as the shear walls in the CFS-NEES Building (Fig. 4f). The backbone points (stress and strain) of the Pinching4 material were as follows: (0.2ε, 0.2V), (0.8ε, 0.8V), (ε,V) and (1.534ε,0.395V). Using the subpanel approach, as introduced by Leng (2015), the whole panel (1 pair of trusses) shear wall model is subdivided into four truss pairs (in this case) in order to facilitate the insertion of non-structural sheathing, as well as, to enable the interaction of shear wall and gravity framing at intermediate locations (Figure 4c, through the two horizontal members). Figure 5 shows the application of this method where the nonlinear response of the subpanel (four truss element pairs) and whole panel (one pair of truss elements) model is compared. It is shown that the models are in good agreement. The post peak response after an approximate displacement of 70mm is due to the fact that the loading exceeded the 4th point displacement inserted in the Pinching 4 material; beyond this point the shear wall specimen has failed. For the shear wall chords a hold-down/chord stud connection was considered. Two zero-length spring elements were attached to the end of the chord studs in the y-direction and a uniaxial parallel material was considered in OpenSees combining the material properties as shown in Figure 4g (Leng 2015). One spring element simulated the tensile strength of the holddown using Pinching4 material with the same compressive and tensile stiffness (F_y = 43.5kN, F_u = 66.75kN, δ_y = 5.94mm, δ_u = 10.51mm for a Simpson S/HDU6 holddown (Simpson Strong-Tie 2017)), while the second spring element incorporated an elastic perfectly plastic gap material with infinite compressive stiffness simulating a pin support for the shear wall chord stud. Information for the nonlinear response of the chord member is provided in Section 3.3.

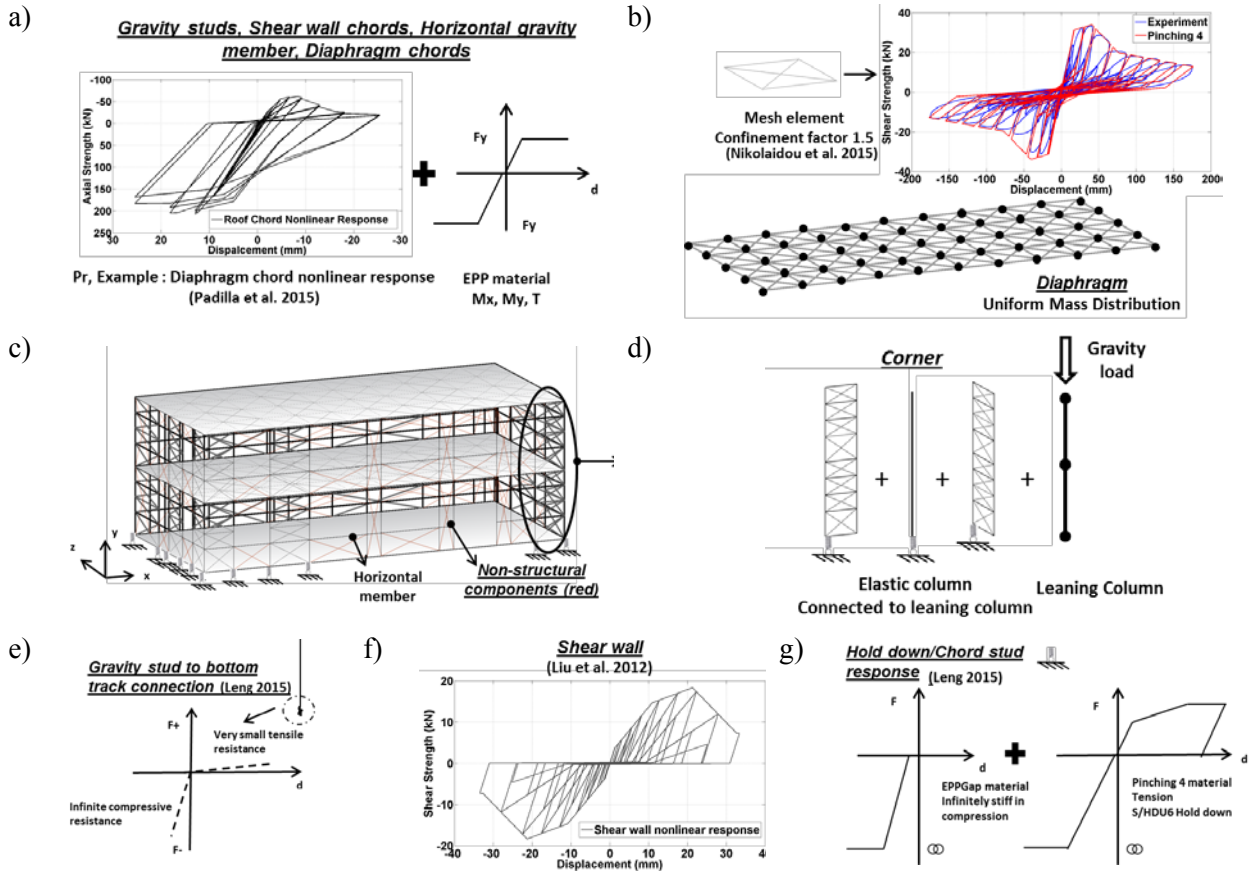

Figure 4. Modelling approach; a) gravity framing, b) diaphragm, c) CFS-NEES Building, d) leaning columns, e) gravity stud – to – bottom track connection, f) shear wall and, g) hold-down/chord stud connection

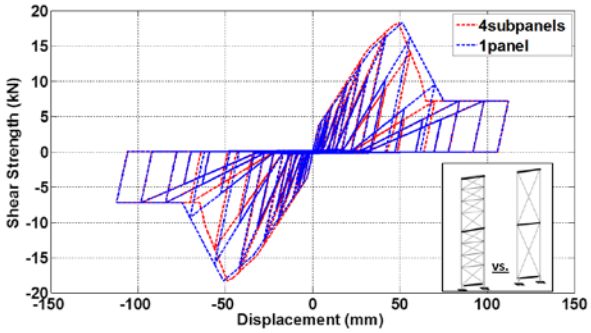

Figure 5. Subpanel approach verification

3.2 Diaphragm simulation

As a first step, the 3.66m × 6.1m diaphragm configurations tested at McGill University were modelled using two Nodelink elements as shown in Figure 6 (a 3.51 × 6.1m 2D Model, without the 152mm sheathing extending inside the wall (Nikolaidou et al. 2017)). Pinching4 parameters were calibrated based on the experimental data, as demonstrated in Figure 4b. Subsequently, a 1.53m × 1.75m mesh element was produced from the 3.51m × 6.1m diaphragm 2D Model in order to model the floor and roof subsystems of the CFS-NEES Building (Figures 4b and 6). Table 2 provides the backbone points and Pinching4 parameters for the mesh elements of the floor and roof subassemblies. An initial comparison with the findings of Chatterjee (2016) and Florig et al. (2015), as described in Section 1, revealed that the shear stiffness values obtained through the diaphragm experimental program at McGill University are lower than the lower bound proposed by Chatterjee. This was attributed to the fact that the ledger framing connection of the diaphragm sheathing to the shear wall studs was not included in the test setup (Figure 1a), while it was part of the work of both Chatterjee and Florig. As such, the shear stiffness of

the floor and roof diaphragms was multiplied with a confinement factor (CF) of 1.5 in order to match, conservatively, the lower bound, as shown in Figures 7a and 7b for both directions of loading; the CF factor represents the influence of the walls stiffness on the diaphragm response. Further study is needed in order to better incorporate this effect. The stiffness and strength of floor and roof in both directions are included in Table 3.

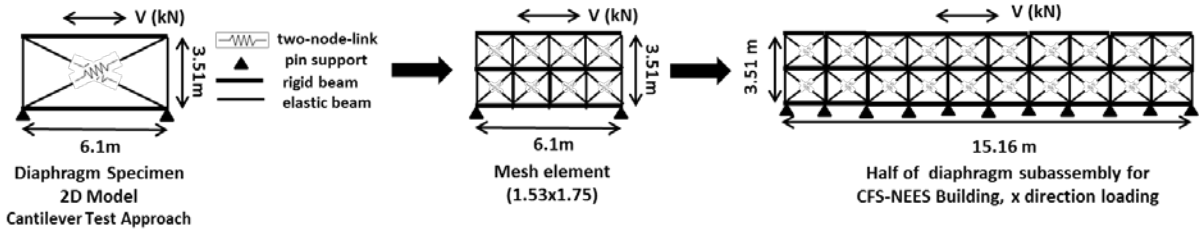

Figure 6. Diaphragm modelling approach

Table 2. Pinching4 material; diaphragm mesh element.

Material parameters	Floor	Roof
±P (kN)	8.4, 8.9, 6.4, 3.4	6, 6.6, 3.9, 2.2
±δ (mm)	4.1, 9.5, 15.6, 49.4	6.8, 13.3, 25.0, 66.3
±rDisp	0.85	0.85
±rForce	0.40	0.40
±uForce	-0.20	-0.20
gk	0.9 0.9 1.2 1.2 0.85	0.9 0.9 1.2 1.2 0.85
gf	0.01 0.05 0.1 0.1 0.90	0.01 0.05 0.1 0.1 0.90
gd	0.2 0.2 2.0 2.0 0.03	0.2 0.2 2.0 2.0 0.03
gE	4.6	4.6

a)

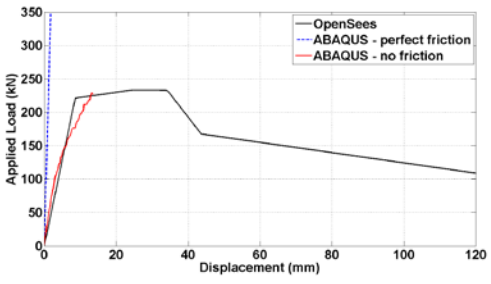

b)

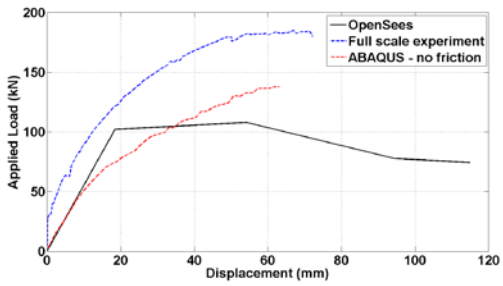

Figure 7. Diaphragm confinement factor (CF); a) long direction, x and, b) short direction, z.

Table 3. Shear strength and stiffness values for floor and roof diaphragm (without CF).

Subsystems	Floor	Roof
$v_{x,z}$ (kN/m)	7.3	5.2
k_x (kN/mm)	17.8	7.6
k_z (kN/mm)	3.5	1.7

3.3 Gravity framing

Given the vast number of CFS members constituting the gravity elements of a CFS structure, half of the gravity studs were included in the simulation of the CFS-NEES Building with their sections doubled in order to compensate for the missing members while simplifying the simulation process. The gravity

members served as supporting members contributing to the lateral stiffness of the structure; gravity load was applied only on the shear walls based on their tributary area and on the four leaning columns placed in the four corners of the structure as shown in Figure 4d. Uniform mass was considered along the diaphragms and wall lines of the structure.

The nonlinear response of shear wall chords, diaphragm chords, rim joists, gravity studs and horizontal members was incorporated combining a Pinching4 material for the axial strength and an elastic perfectly plastic material for the bending strength and torsional stiffness. All members were considered braced against global buckling modes. The sections were the following: 600s162-54/33 floor/roof gravity studs, double 600s162-54 shear wall chord members, 1200s200-54 roof joists, 1200t200-68 roof rim joists, 1200s250-97 floor joists, 1200t200-97 floor rim joists and 600t150-54 horizontal members (Peterman 2014). The Pinching4 material backbone points and unloading – reloading pinching parameters were calculated as a function of the local buckling slenderness using the analytical expressions, as provided in Tables 7.3, 7.7, 7.8 and 7.9 in Padilla-Liano's thesis (2016). It should be noted that Padilla-Liano's work is a first attempt in characterizing the nonlinear behaviour of CFS studs. The direct strength method (AISI S100 (2016), Schafer (2010)) was employed for the calculation of the member capacities as shown in Table 4.

The gravity stud connection to the bottom track of the structure has no uplift stiffness (Leng 2015); thus a multilinear material was inserted in a zero-length spring with infinite compressive stiffness and negligible tensile stiffness, as shown in Figure 4e.

Table 4. Gravity framing; member capacities

Member Capacities	**Double 600s162-54**	**Double 600s162-33**	**1200t200-97**	**1200s250-97**	**1200t200-68**	**1200s200-54**	**600t150-54**
P+ (kN)	293.55	113.33	363.86	461.76	294.48	248.48	132.96
P- (kN)	-133.34	-42.10	-135.15	-190.66	-82.24	-65.46	-51.72
M_x(kNm)	8.2	3.1	15.0	28.1	11.7	10.4	3.4
M_y(kNm)	±1.82	±0.7	1.2/-1.3	2.6/-3.2	0.8/-1.2	1.0/-1.9	±0.4

3.4 Nonstructural components

Nonstructural interior gypsum sheathing is typically installed along the shear walls and gravity walls of a CFS structure. Exterior OSB sheathing is also installed on the gravity walls. For both shear and gravity walls, OSB and gypsum sheathing was simulated using only one pair of truss elements for each part of the wall, as shown in Figure 4c (in red), with Pinching4 material parameters incorporating the combined action of the two in both sides of the wall. For the shear walls the experimental nonlinear response of Tests 3 & 13 from Liu's work (2012) was used to calibrate the Pinching4 parameters, similarly as explained in Section 3.1. These shear wall specimens had both OSB and gypsum sheathing during testing. For the gravity walls there are no experimental data available at present. Leng (2015) used a fastener based model introduced in the work of Bian et al. (2015) and Buonopane et al. (2015) and provided two separate monotonic nonlinear responses for a 2.44m × 2.74m gravity wall with OSB and one with gypsum sheathing. Summing up the two nonlinear responses led to a combined nonlinear response for a gravity wall with both OSB and gypsum, which was used to produce the backbone points for the Pinching4 material. This summation method was suggested by Chen et al. (2014) for timber shear walls. To further verify this method, a small 2D shear wall model was created; Liu's tests 12 (only OSB) and 16 (only gypsum) were incorporated in the model using two pairs of coincident truss elements. The lateral response of this model was compared to that of a shear wall model with the same structural characteristics and only one pair of truss elements incorporating the response of Liu's Test 13 (both OSB and gypsum). In Figure 8a, it is demonstrated that the two models are in good agreement. Figure 8b shows a comparison of the lateral response of a two-pair shear wall model incorporating separately Leng's nonlinear responses compared to a one-pair shear wall model incorporating the combined calculated nonlinear response (summed up). The unloading-reloading pinching parameters were the same for the gravity walls as for the shear walls. The subpanel approach was used for gravity walls of

various widths and heights.

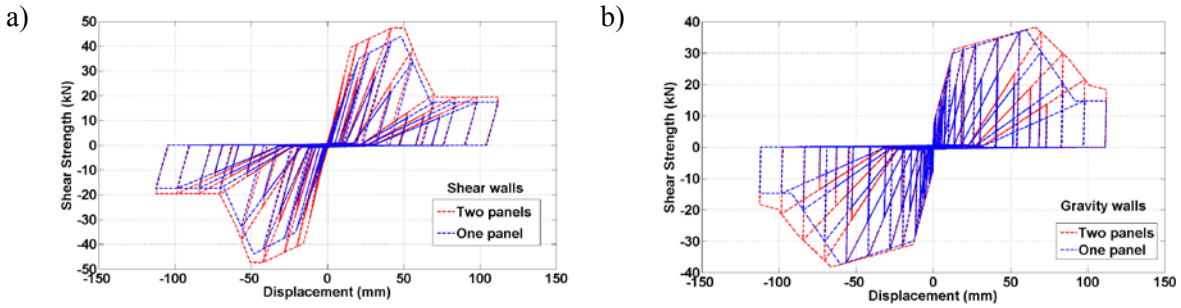

Figure 8. Nonstructural components; a) shear walls and, b) gravity walls.

4. RESULTS

Response history analysis was conducted for the Canoga Park (CNP) (100%) ground motion (design level earthquake in the USA), which was the ground motion applied for the Phase1 of testing. Results are presented for the CFS-NEES Building considering only structural components (Phase 1/2a of testing, Peterman 2014) and, subsequently, the nonstructural components are added to the model (Phase 2c) and their effect on the seismic response of the structure is quantified.

4.1 Phase 1/2a

The first step in understanding the seismic response of a CFS structure is the verification of the simulation approach using the experimental data as provided in Peterman (2014) for the CFS-NEES Building. Tables 5 and 6 include a comparison in the form of fundamental period, wall line inter-storey drift ratios, the maximum diaphragm deflection in the z direction (MDD_z) and the maximum total displacement (shear walls and diaphragm) at the floor level, as well as base shear forces in the two directions, as recorded considering only the shear wall forces. All three components of the CNP ground motion were applied (x, y and z). Figures 9a and 9b include also a comparison of the wall-line inter-storey drift ratios in the x-direction in the floor and roof level. It is shown that, although more flexible, the model is able to adequately predict the global seismic response of the building.

Table 5. Fundamental periods and wall line inter-storey drift ratios, Phase 1; Comparison

Phase 1	**Δ_{u1}/h(%)**	**Δ_{u2}/h(%)**	**Δ_{v1}/h(%)**	**Δ_{v2}/h(%)**	**T_x**	**T_z**
Model	1.54	1.18	0.74	0.51	0.34	0.39
Test	1.18	0.81	0.85	0.56	0.31	0.36

Note: The drift was calculated based on the average displacement of two corner nodes in each direction (u for x direction and v for z direction)

Table 6. MDD_z , maximum floor displacement and base shear force, Phase 1; Comparison

Phase 1	**V_x (kN)**	**V_z (kN)**	**Max Displacement (mm)**	**MDD_z (mm)**
Model	91.9	61.4	27.4	7.5
Test	84.4*	79.1*	28	3.5

*Note: Based on Peterman (2014) using Method 1 (equivalent lateral force procedure).

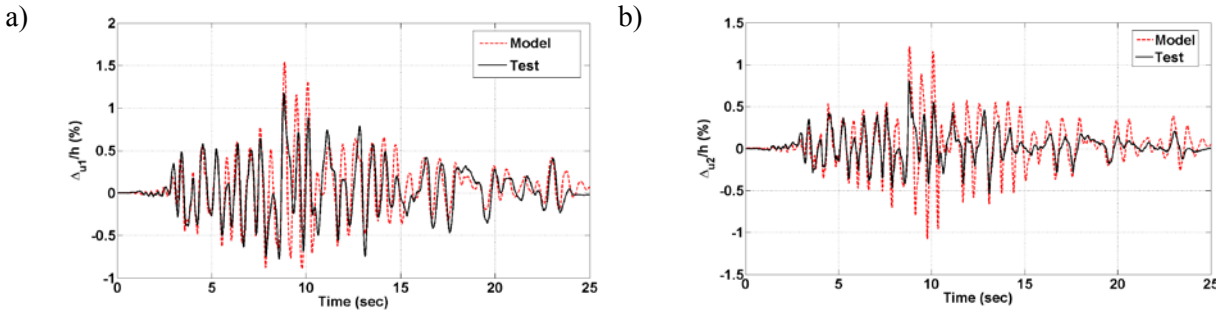

Figure 9. Wall line inter-storey drift ratios, x-direction; a) floor level and, b) roof level.

4.2 Phase 2c

The non-structural gypsum and gravity walls were added to the model, as explained in Section 3.4, and the CNP (100%) ground motion was applied considering now only the x and z components of the earthquake.

Table 7. Phase 1/2a vs. 2c, Fundamental period and wall line inter-storey drift ratios.

Model	**T_x (sec)**	**T_z(sec)**	**Δ_u/h(%),Floor**	**Δ_u/h(%),Roof**	**Δ_v/h(%),Floor**	**Δ_v/h(%),Roof**
Phase 1/2a	0.34	0.39	1.54	1.18	0.74	0.51
Phase 2c	0.21	0.31	0.65	0.33	0.41	0.25
Comp (%)	38	21	58	72	45	51

Table 8. Phase 1/2a vs. 2c, MDD_z, maximum floor displacement and base shear.

Model	**MDD_z (mm)**	**Max Displacement (mm)**	**V_x (kN)**	**V_z (kN)**
Phase 1/2a	7.5	27.4	143.9	98.9
Phase 2c	8.2	19	261	129
Comp (%)	9	31	81	30

Note: Base shear forces from shear walls and gravity framing for only the x and z direction CNP components.

In Table 7 it is shown that the addition of the non-structural gypsum and gravity walls led to a much stiffer structure with an average reduction of the fundamental periods by 30% and an over 50% decrease of the wall line inter-storey drift ratios. Accordingly, there was a 9% increase of the MDD_z for the floor diaphragm with a 31% decrease of the total floor displacement given that the gypsum panels increased the shear wall stiffness by approximately 20% and the gravity walls contributed in the lateral stiffness of the wall lines (Table 8). As expected, the base shear forces increased in both directions and, most prominently, in the x-direction given the large number of truss elements added in the x direction wall lines (Figure 4c, Table 8). It was observed that shear wall forces were reduced by 27 % in the x-direction and 15% in the z-direction, respectively, with the gravity walls now receiving 75% and 62% of the base shear in the x- and z- direction, respectively. It is shown that with the addition of OSB and gypsum panels the gravity walls in Phase 2c attain a primary role as lateral force resisting elements, while in Phase 1/2a the primary lateral force resisting elements were the shear walls (~ 60% of base shear).

5. CONCLUSIONS

The study presented herein aims to clarify the importance of non-structural components for the lateral response of CFS structures in a subsystem and system level. In the first part of the paper, it is shown that the addition of non-structural gypsum ceiling and gypcrete topping leads to an over 100% increase in shear stiffness and a minimum 60% increase of shear strength for a CFS framed / OSB sheathed diaphragm subsystem. In the second part, the CFS-NEES Building is modelled following a simplified approach, which is verified using experimental data. The addition of non-structural gypsum and exterior OSB all along the wall lines results in a much stiffer structure with the gravity walls becoming the

primary lateral force resisting elements. This highlights the need for the non-structural components to be included in the seismic design provisions for CFS structures.

6. ACKNOWLEDGMENTS

The authors appreciate greatly the information and data provided by Professor Benjamin W. Schafer and Dr. Cristopher D. Moen, as well as Dr. Kara Peterman, Dr. Aritra Chatterjee, Dr. Jiazhen Leng and Dr. David A. Padilla-Liano related to the CFS-NEES Building. The authors would also like to thank the Natural Sciences and Engineering Research Council of Canada (NSERC), as well as, the American Iron and Steel Institute (AISI) and the Canadian Sheet Steel Building Institute (CSSBI) for financially supporting this research project.

7. REFERENCES

Accorti M, Baldassino N, Zandonini R, Scavazza F, Rogers CA (2016). Response of CFS sheathed shear walls. *Structures;* 7 100-112.

AISI S100 (2016). North American specification for the design of cold - formed steel structural members. *American Iron and Steel Institute*, Washington, USA.

AISI S400 (2015). North American standard for seismic design of cold-formed steel structural systems. *American Iron and Steel Institute*, Washington, USA.

Branston AE, Boudreault FA, Chen CY, Rogers CA (2006). Light-gauge steel-frame wood structural panel shear wall design method. *Canadian Journal of Civil Engineering*; 33(7) 872-889.

Bian G, Padilla-Llano DA, Leng J, Buonopane SG, Moen CD, Schafer BW (2015). OpenSees modeling of cold formed steel framed wall system. *Proceedings of 8th International Conference on Behavior of Steel Structures in Seismic Areas*, Shanghai, China.

Buonopane SG, Bian G, Tun TH, Schafer BW (2015). Computationally efficient fastener-based models of cold-formed steel shear walls with wood sheathing. *Journal of Constructional Steel Research*; 110 137-148.

Chatterjee A (2016). Structural system reliability with application to light steel-framed buildings. *PhD Thesis*, Department of Civil Engineering, Virginia Polytechnic Institute and State University, Blacksburg, USA.

Chen Z, Nott A, Chui YH, Doudak G, Ni C, Mohammad M (2014). Experimental study on the contribution of GWB to the lateral performance of wood shear walls. *World Conference on Timber Engineering*, Quebec City, Canada.

CSA S136 (2016). North American specification for the design of cold-formed steel structural members. *Canadian Standards Association*, Rexdale, Canada.

Dubina, D (2008). Behavior and performance of cold-formed steel-framed houses under seismic action. *Journal of Constructional Steel Research*; 64 896–913

Fiorino L, Iuorio O, Macillo V, Landolfo R (2012). Performance-based design of sheathed CFS buildings in seismic area. *Thin - Walled Structures*; 61 248–257.

Florig S, Chatterjee A, O'Brien P, Moen CD (2015). Full scale tests on a cold-formed steel floor diaphragm with oriented strand board sheathing. *Report No. CE/VPI-ST-16/02*, American Iron and Steel Institute, Washington, USA.

Krawinkler H, Parisi F, Ibarra L, Ayoub A, Medina R (2000). Development of a testing protocol for wood frame structures. Report W-02 covering Task 1.3.2, CUREE/Caltech Woodframe Project. Consortium of Universities for Research in Earthquake Engineering (CUREE), Richmond, USA.

Latreille P (2016). Characterization of wood sheathed cold-formed steel diaphragms under in plane loading (Phase 2 of diaphragm research program). *Master's Thesis*, Department of Civil Engineering, McGill University, Montreal, Canada.

Liu P, Peterman KD, Yu C, Schafer BW (2012). Cold-formed steel shear walls in ledger-framed buildings. *Annual Stability Conference,* Structural Stability Research Council, Grapevine, USA.

Leng J (2015). Simulation of cold-formed steel structures. *PhD Thesis*, Department of Civil Engineering, Johns Hopkins University, Baltimore, USA.

Lowes LN, Altoontash A (2003). Modeling reinforced-concrete beam-column joints subjected to cyclic loading. *Journal of Structural Engineering*; 129(12) 1686-1697.

Lu S (2015). Influence of gypsum panels on the response of cold-formed steel framed shear walls. *Master's Thesis*, Department of Civil Engineering, McGill University, Montreal, Canada.

McKenna F (1997). Object-oriented finite element programming: Frameworks for analysis, algorithms, and parallel computing. *PhD Thesis*, Department of Civil Engineering, University of California, Berkeley, USA.

Nikolaidou V, Latreille P, Rogers CA, Lignos DG (2017). Seismic performance characterization of wood-Sheathed and cold-formed steel framed floor and roof diaphragm structures. *Journal of Structural Engineering*, American Society of Civil Engineers, Reston, USA. (In press)

Padilla-Liano D (2015). A framework for cyclic simulation of thin-walled cold-formed steel members in structural systems. *PhD Thesis*, Department of Civil Engineering, Virginia Polytechnic Institute and State University, Blacksburg, USA.

Pan CL, Shan MY (2011). Monotonic shear tests of cold-formed steel wall frames with sheathing. *Thin-Walled Structure*; 49(2) 363-370.

Peterman KD (2014). Behavior of full-scale cold-formed steel buildings under seismic excitations. *PhD Thesis*, Department of Civil Engineering, Johns Hopkins University, Baltimore, USA.

Schafer BW (2010). Review: the direct strength method of cold-formed steel member design. *Journal of Constructional Steel Research*; 64(7) 766-778.

Shamim I (2012). Seismic design of lateral force resisting cold-formed steel framed (CFS) structures. *PhD Thesis*, Department of Civil Engineering, McGill University, Montreal, Canada.

Shamim I, DaBreo J, Rogers CA (2013). Dynamic testing of single-and double-story steel-sheathed cold-formed steel-framed shear walls. *Journal of Structural Engineering*; 139(5) 807-817.

Shamim I, Rogers CA (2015). Numerical evaluation: AISI S400 steel-sheathed CFS framed shear wall seismic design method. *Thin-Walled Structures*; 95 48-59.

Simpson Strong-Tie Company Inc. (2017). Connectors for cold-formed steel construction: S/HDU Holdowns. Pleasanton, USA.

Yu C, Li C. (2012). Experimental investigation of cold-formed steel shear walls sheathed with steel-gypsum composite panels. *Annual Stability Conference,* Structural Stability Research Council, Grapevine, USA.